A dynamic wall model for Large-Eddy simulations of wind turbine dedicated airfoils.

Calafell J.[1,2]**,Lehmkuhl O.**[1,2]**, Carmona A.**[1]**, Pérez-Segarra C.D.**[1] **and Oliva A.**[1]

[1] Heat and Mass Transfer Technological Center, Polytechnical University of Catalonia (UPC), Colom 11, 08222 Terrassa (Barcelona)
[2] Termo Fluids, S.L., Av. Jacquard 97-E, 08222 Terrassa (Barcelona)

E-mail: joancs@cttc.upc.edu

Abstract. This work aims at modelling the flow behavior past a wind turbine dedicated airfoil at high Reynolds number and large angle of attack (AoA). The DU-93-W-210 airfoil has been selected. To do this, Large Eddy Simulations (LES) have been performed. Momentum equations have been solved with a parallel unstructured symmetry preserving formulation while the wall-adapting local-eddy viscosity model within a variational multi-scale framework (VMS-WALE) is used as the subgrid-scales model. Since LES calculations are still very expensive at high Reynolds Number, specially at the near-wall region, a dynamic wall model has been implemented in order to overcome this limitation. The model has been validated with a very unresolved Channel Flow case at $Re_\tau = 2000$. Afterwards, the model is also tested with the Ahmed Car case, that from the flow physics point of view is more similar to an stalled airfoil than the Channel Flow is, including flow features as boundary layer detachment and recirculations. This case has been selected because experimental results of mean velocity profiles are available. Finally, a flow around a DU-93-W-210 airfoil is computed at $Re = 3 \times 10^6$ and with an AoA of 15°. Numerical results are presented in comparison with Direct Numerical Simulation (DNS) or experimental data for all cases.

1. Introduction

The flow around aerodynamic profiles in pre- or full-stall at high Reynolds numbers is a problem of increasing interest since it is a normal operation state for wind turbine blades. In the past years, it has been subject of many experimental and numerical investigations. Most of the numerical studies performed since now have been carried out using RANS modelling, but it is well-known that such models fails in predicting the flow at angles of attack near or after stall, mainly due to the highly unsteady and three-dimensionality nature of the flow. Under these situations, large-eddy simulations (LES) can be a good alternative for simulating such complex flows. However, at present LES calculations are still prohibitively expensive at high Reynolds Number, specially for aerodynamic applications where wall flows are present.

Different strategies can be found in the literature in order to reduce mesh requirements at the near-wall region such as hybrid Reynolds Averaged Navier Stokes (RANS)/LES approach or Wall Functions. Dynamic wall models in which this paper is focused, are part of these strategies. All wall models in which the near wall velocity field is obtained through the resolution of flow governing equations are included in the category of dynamic models.

The proposed formulation is based on the full RANS equations resolution so, the near wall flow field has a much low approximation level if compared with other strategies like wall functions or other dynamic wall models. In wall functions, near wall mean velocity profiles obtained from canonic flows are used to calculate the wall shear stress while in the dynamic wall model proposed by Wang and Moin [1], turbulent boundary layer equations are solved instead of full Navier Stokes. This lower degree of approximation leads to a more general method.

The present model is intended to make feasible calculations of industrial applications that are computationally prohibitive until now . Since complex geometries are found in most these applications, the model has been formulated for unstructured meshes. In the present work, the model is tested with a very unresolved Channel Flow case at $Re_\tau = 2000$ and with an Ahmed Car test at $Re = 7 \times 10^5$. Comparison with DNS and experimental results will allow us to validate the numerical formulation. Once the model is validated, it is used together with an LES model to calculate a flow past a DU-93-W-210 airfoil.

A parallel unstructured symmetry preserving formulation has been used to solve momentum equations while the wall-adapting local-eddy viscosity model within a variational multi-scale framework (VMS-WALE) has been applied to model subgrid scales (SGS). This model has been proved to perform well on unstructured grids [2]. The study has been carried out for Reynolds numbers of 3×10^6 and an AoA of 15°. Numerical results using and not using the dynamic wall model have been compared with experimental ones.

2. Mathematical and numerical formulation of the LES

The turbulent flow is described by means of LES using symmetry-preserving discretizations. The spatial filtered and discretized Navier-Stokes equations can be written as,

$$\mathsf{M}\boldsymbol{u} = 0 \tag{1}$$

$$\Omega\frac{\partial\overline{\boldsymbol{u}}}{\partial t} + \mathsf{C}\left(\overline{\boldsymbol{u}}\right)\overline{\boldsymbol{u}} + \nu\mathsf{D}\overline{\boldsymbol{u}} + \rho^{-1}\Omega\mathsf{G}\overline{\boldsymbol{p}} \;=\; \mathsf{C}\left(\overline{\boldsymbol{u}}\right)\overline{\boldsymbol{u}} - \overline{\mathsf{C}\left(\boldsymbol{u}\right)\boldsymbol{u}} \;\approx\; -\mathcal{M}\mathcal{T}_m \tag{2}$$

where M, C, D and G are the divergence, convective, diffusive and gradient operators, respectively, Ω is a diagonal matrix with the sizes of control volumes, ρ is the fluid density, ν the viscosity, $\overline{\boldsymbol{p}}$ represents the filtered pressure, $\overline{\boldsymbol{u}}$ is the filtered velocity, $\mathcal{M}$ represents the divergence operator of a tensor, and $\mathcal{T}_m$ is the SGS stress tensor, which is defined as,

$$\mathcal{T}_m = -2\nu_{sgs}\overline{\mathcal{S}} + (\mathcal{T}_m : \mathsf{I})\mathsf{I}/3 \tag{3}$$

where $\overline{\mathcal{S}} = \frac{1}{2}[\mathsf{G}(\overline{\boldsymbol{u}}) + \mathsf{G}^*(\overline{\boldsymbol{u}})]$. To close the formulation, a suitable expression for the SGS viscosity, ν_{sgs}, must be introduced. In the present work the Smagorinsky (SMG), the WALE and the VMS-WALE models have been used to evaluate ν_{sgs}. For the sake of brevity, only the VMS-WALE model is defined below. The standard implementations of the Smagorinsky [3] and WALE [4] models are used in the present work while new features that are worth to be described are included in the VMS-WALE model. In the variational multiscale (VMS) approach [5], originally formulated for the Smagorinsky model by Hughes in the Fourier space, three classes of scales are considered: large, small and unresolved scales [6]. Thus, for the large-scale parts of the resolved $\overline{\boldsymbol{u}}$ a general governing equation can be derived,

$$\Omega\frac{\partial\overline{\boldsymbol{u}}}{\partial t} + \mathsf{C}\left(\overline{\boldsymbol{u}}\right)\overline{\boldsymbol{u}} + \nu\mathsf{D}\overline{\boldsymbol{u}} + \rho^{-1}\Omega\mathsf{G}\overline{\boldsymbol{p}} \;=\; -\frac{\partial\widehat{\mathcal{T}}}{\partial x_j} - \frac{\partial\mathcal{T}'}{\partial x_j} \tag{4}$$

Inspecting equation 4 it is possible to identify $\widehat{\mathcal{T}}$ as the subgrid term in the large-scale equation and $\mathcal{T}'$ as the subgrid small-scale term. Now, neglecting the effect of unresolved scales in the

large-scale equation ($\widehat{\mathcal{T}} \approx 0$) , we only need to model the $\mathcal{T}'$. In our implementation the *small-small* strategy is used in conjunction with the WALE model:

$$\begin{aligned}
\mathcal{T}' &= -2\nu_{sgs}\mathcal{S}_{\mathrm{ij}}{}' + \frac{1}{3}\mathcal{T}'\delta_{ij} \\
\nu_{sgs} &= (C_w^{vms}\Delta)^2 \frac{(\mathcal{V}_{\mathrm{ij}}{}' : \mathcal{V}_{\mathrm{ij}}{}')^{\frac{3}{2}}}{(\mathcal{S}_{\mathrm{ij}}{}' : \mathcal{S}_{\mathrm{ij}}{}')^{\frac{5}{2}} + (\mathcal{V}_{\mathrm{ij}}{}' : \mathcal{V}_{\mathrm{ij}}{}')^{\frac{5}{4}}} \\
\mathcal{S}_{\mathrm{ij}}{}' &= \frac{1}{2}[\mathsf{G}(\overline{\boldsymbol{u}'}) + \mathsf{G}^*(\overline{\boldsymbol{u}'})] \\
\mathcal{V}_{\mathrm{ij}}{}' &= \frac{1}{2}[\mathsf{G}(\overline{\boldsymbol{u}'})^2 + \mathsf{G}^*(\overline{\boldsymbol{u}'})^2] - \frac{1}{3}(\mathsf{G}(\overline{\boldsymbol{u}'})^2\mathsf{I})
\end{aligned} \tag{5}$$

where C_w^{vms} is the equivalent of the WALE coefficient for the *small-small* VMS approach and in the finite volume context its value lies in the range between 0.3 and 0.5. In our studies a value of 0.325 is used.

The governing equations have been discretized on a collocated unstructured grid arrangement by means of second-order spectro-consistent schemes [7]. Such schemes are conservative, i.e. they preserve the symmetry properties of the continuous differential operators and ensure both, stability and conservation of the kinetic-energy balance even at high Reynolds numbers and with coarse grids. These conservation properties are held if, and only if the discrete convective operator is skew-symmetric ($\mathsf{C}(\boldsymbol{u}) = -\mathsf{C}^*(\boldsymbol{u})$), the negative conjugate transpose of the discrete gradient operator is exactly equal to the divergence operator ($-(\Omega\mathsf{G})^* = \mathsf{M}$) and the diffusive operator D, is symmetric and positive-definite. For the temporal discretization of the momentum equation a two-step linear explicit scheme on a fractional-step method has been used for the convective and diffusive terms, while for the pressure gradient term an implicit first-order scheme has been used. This methodology has been previously used with accurate results for solving the flow over bluff bodies with massive separation [2, 8, 9].

3. The Dyamic Wall Model

The dynamic wall model (DWM) is based on the implicit resolution of the full spatial discretized RANS equations (6) in a fine embedded mesh called wall domain mesh (WDM). The WDM is generated by extrusion of the superficial mesh of the solid face between the wall and the first off-wall node of the LES mesh (LDM) [1].

$$\Omega\frac{\partial\langle\boldsymbol{u}\rangle}{\partial t} + \mathsf{C}(\langle\boldsymbol{u}\rangle)\langle\boldsymbol{u}\rangle = \mathcal{M}[2(\nu+\nu_T)\langle\mathcal{S}\rangle] - \rho^{-1}\Omega\mathsf{G}\langle\boldsymbol{p}\rangle \tag{6}$$

where M, C and G are the divergence, convective, and gradient operators respectively, $\langle\mathcal{S}\rangle$ is the strain rate tensor, Ω is a diagonal matrix with the sizes of control volumes, ρ is the fluid density, ν the viscosity, ν_T the turbulent RANS viscosity and finally, $\langle\boldsymbol{p}\rangle$ and $\langle\boldsymbol{u}\rangle$ the time averaged pressure and velocity respectively.

The equations are solved numerically by means the finite volume method. Symmetry preserving numerical schemes have been used to carry out the spatial discretization of the convective term, while second order central difference scheme has been applied for the diffusive one. In order to solve the velocity-pressure coupling, an implicit projection method has been implemented.

Regarding the boundary conditions, Dirichlet ones are prescribed at the outer surface for velocities and pressure taking its values from the LES domain, while at the solid face, no-slip and Neumann conditions are applied for velocities and pressure respectively. Finally, if side boundaries do exist, the same boundary conditions than LES domain are applied to them. In figure 1, the WDM geometry is shown.

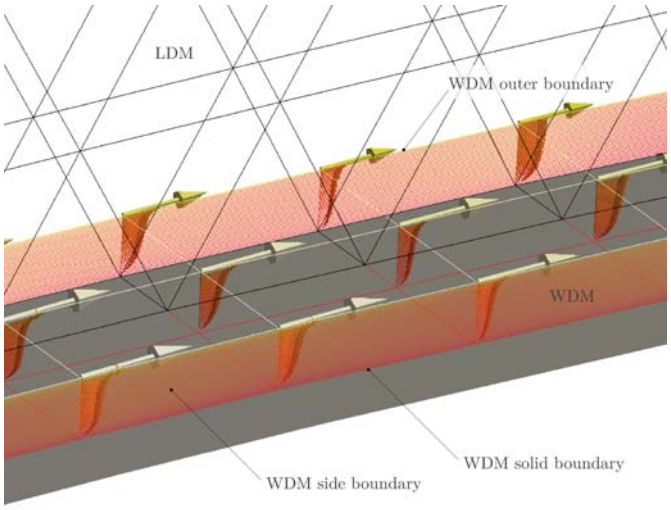

Figure 1. Dynamic wall model scheme. The WDM is embedded into the LDM.

The RANS equations turbulent eddy viscosity (ν_T) is obtained according the Spalart-Allmaras model, a one-equation RANS model suitable for wall bounded flows [10].
Once the mean velocity field is obtained, an accurate mean wall shear stress can be computed according the following expression:

$$\tau_{wi} \approx (\mu + \mu_T)\frac{u_{iy1}}{\delta_{y_1}} \tag{7}$$

Where τ_{wi} is the i^{th} component of the shear stress related to a local coordinate system parallel to the solid surface ij, μ is the local viscosity, μ_T is the local turbulent viscosity, u_{iy1} is the i^{th} component of the velocity corresponding to the first off-wall node of the WDM, and δ_{y_1} is the distance between the node and the wall. At the LES domain, slip and Neumann boundary conditions are applied at the solid faces for velocity and pressure respectively. The calculated τ_w value is used to evaluate the slip velocity at the wall. This ensures that the LES-domain calculated τ_w matches the wall model value when evaluating the diffusive term.

The main advantage of this methodology arises from the fact that the explicit LES-domain mesh is much coarser than the implicit RANS/wall-domain one. Hence, despite that the wall model equations are solved at every LES iteration, a much bigger time step can be used compared to the one that should be taken if the LDM size were of the same order of magnitude than the WDM one.

4. The model performance evaluation: The Channel Flow test.

The main objective of this section is not to obtain a very well resolved Channel Flow but to evaluate how the model is able to compute a correct value of wall shear stress, and how this value, once introduced in the LES domain helps to improve the overall results. To do so, a very coarse mesh of 68x33x34 control volumes has been used. Periodic conditions have been prescribed in all directions except in the upper and lower walls where slip wall conditions have been applied. Two different turbulence models have been used for the LES domain, the VMS-WALE and the Smagorinsky one. In cases where the dynamic wall model has been used, the WDM has been extruded in 40 layers.

A high Reynolds number of $Re_\tau = 2000$ has been selected in order to challenge the wall model. According to the empirical expression $Re_\tau = 0.09Re_m^{0.88}$ [11] this value of Re_τ is equivalent to

$Re_m = 87002.4$. Re_m is defined as $2\delta\overline{U}/\nu$ where δ is the channel half height, $\overline{U}$ is the bulk velocity and ν is the kinematic viscosity of the fluid.

From general turbulence theory, an expression derived from the stream-wise mean momentum equation, states that the wall shear stress and the pressure gradient in the flow direction are related as follows [11]:

$$-\frac{dp_w}{dx} = \frac{\tau_w}{\delta} \tag{8}$$

The strategy is based on prescribing a calculated pressure gradient evaluated from Re_τ by using equation 8 and checking if the calculated numerical value of Re_τ matches the value initially used to determine the imposed pressure gradient. Hence, the capabilty of computing an accurate wall shear stress is evaluated by proving that the numerical solution matches the analytic one by means the value of Re_τ as it is a direct function of τ_w. In table 1, the Re_τ calculated by using and not using the dynamic wall model, are compared with the expected value (the one used to evaluate dp_w/dx).

Finally, in order to check the improvement of the numerical results of the LES domain, the values obtained with the dynamic wall model and those obtained without it, will be compared with DNS data [12] and the law of the wall. This law describes the mean velocity profile in the flow direction as a function of the distance to the wall [11]: $u^+ = y^+$ if $y^+ < 5$ (i.e. the viscous sublayer) and $u^+ = (1/\kappa)\ln y^+ + B$ if $y^+ > 30$ (i.e. the log-law region). The superindex $^+$ denotes that the variable is in wall units while u^+ is the stream-wise mean velocity, y^+ is the wall distance, k is the von Kármán constant ($k = 0.41$), and B is a constant whose value for the channel flow is $B = 5.2$. As a mesure of the mesh coarseness, at $Re_\tau = 2000$ the first off-wall node of the LDM is located at $y^+ = 60.606$, it is far above the viscous sublayer and well into the logarithmic law region.

4.1. The Channel Flow test results.

In table 1 a comparison between the reference values of Re_τ and the calculated numerical results is shown. The numerical results have been obtained with and without wall model in order to check the model improvements to the Re_τ evaluation. Regarding the LES domain, two different LES models have been used in order to evaluate the interaction between the dynamic wall and the LES. In the present work, the Smagorinsky and the VMS-WALE have been used.

Table 1. Comparison between the reference Re_τ value, and the numerical results calculated with and without the dynamic wall model by means two different LES models.

LES turb. model	ref. Re_τ	Re_τ w/o model	rel. err.[%]	Re_τ w/ model	rel. err.[%]
Smagornisky	2000.0	2031.6	1.58	2017.26	0.86
VMS-WALE	2000.0	1849.4	7.52	1996.89	0.15

Regarding the mean velocity profiles, in figures 2 and 3, the mean stream-wise velocity component is plotted in wall units as a function of the wall distance that is represented in logarithmic scale. Numerical results obtained with the VMS-WALE and the Smagorinsky models are displayed toghether with DNS data in figures 2 and 3 respectively. The law of the wall is also displayed in the figures. Between $y^+ = 0$ and $y^+ = 5$ the viscous sublayer behavior is plotted while for values higher than $y^+ = 30$ the logarithmic law is shown. On the other hand, in figures 4 and 5, the obtained fluctuations of the stream-wise velocity component are plotted together with the DNS reference. For both LES models, computations with and without DWM have been carried out and plotted to evaluate the model effects.

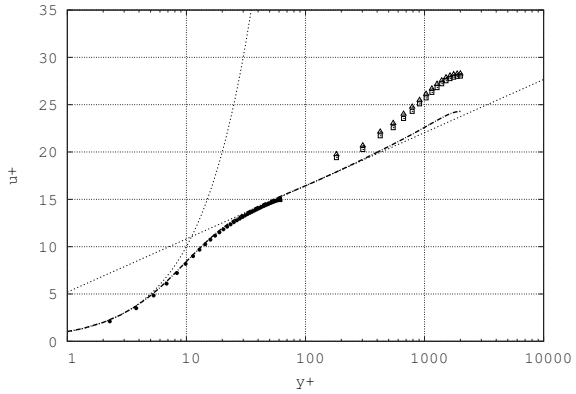

Figure 2. Mean velocity profiles of the stream-wise velocity component vs. wall distance at $Re_\tau = 2000$ and VMS-WALE as a LES model. All variables are in wall units and x-axis is represented in logarithmic scale. ● DWM profile, □ LES w/ wall model, △ LES w/o wall model, ····· wall law, — · —DNS.

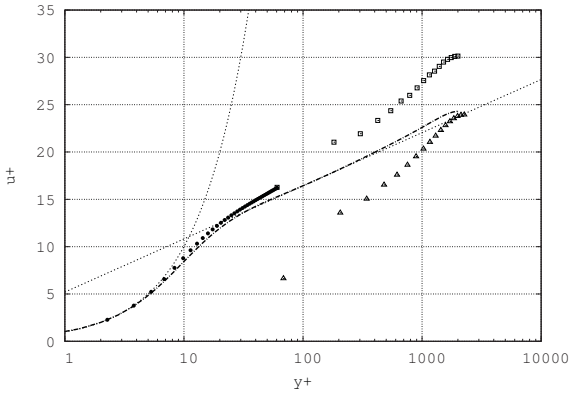

Figure 3. Mean velocity profiles of the stream-wise velocity component vs. wall distance at $Re_\tau = 2000$ and Smagorinsky as a LES model. All variables are in wall units and x-axis is represented in logarithmic scale. ● DWM profile, □ LES w/ wall model, △ LES w/o wall model, ····· wall law, — · —DNS.

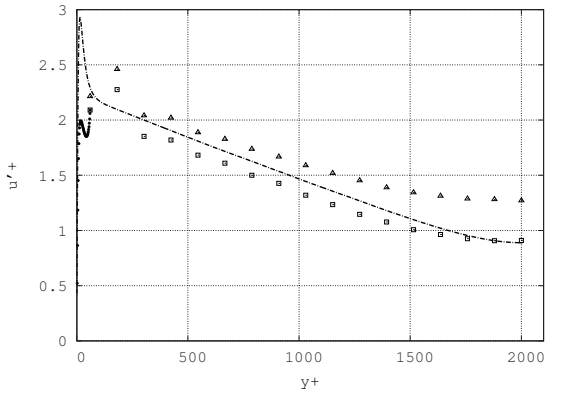

Figure 4. Fluctuations of the stream-wise velocity component vs. wall distance at $Re_\tau = 2000$ and VMS-WALE as a LES model. All variables are in wall units. ● DWM profile, □ LES w/ wall model, △ LES w/o wall model, — · —DNS.

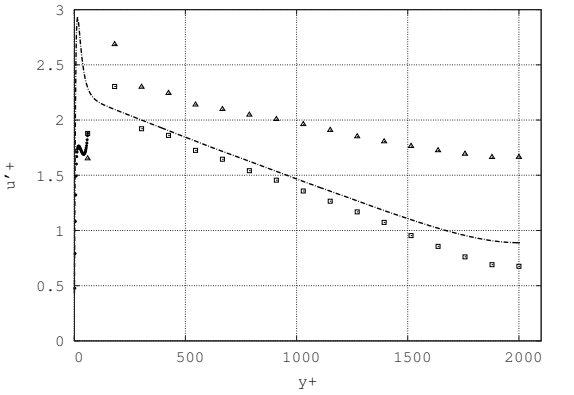

Figure 5. Fluctuations of the stream-wise velocity component vs. wall distance at $Re_\tau = 2000$ and Smagorinsky as a LES model. All variables are in wall units. ● DWM profile, □ LES w/ wall model, △ LES w/o wall model, — · —DNS.

4.2. Conclusions from the Channel Flow test.

While the first off-wall node of the LDM is located at $y^+ = 60.606$, the first node of the WDM is at $y^+ = 0.757$ lying well into the viscous sublayer. The velocity profile in this region is linear and that allows an accurate computation of the wall shear stress as it can be observed in table 1. Errors in the calculation of Re_τ are quite lower when calculated through the wall model for the VMS-WALE case. It has to be taken into account that the objective of these calculations was not to obtain a well resolved Channel Flow. Instead, the main target was to evaluate the improvement of the numerical results with respect to a reference when using the

dynamic wall model. Regarding the mean velocity profiles, an improvement in the LES domain is observed, specially in the case of the Smagorinsky model while in the DWM domain, the profiles match almost exactly the DNS data. When it comes to the velocity fluctuations, a very significant improvement is observed in the LES domain for both subgrid models. It is not the case in the DWM domain. These results were expected taking into account the inablity of RANS models to predict velocity fluctuations properly. However the main target of improving the LES results was achieved. Despite the different time scales between LES and RANS domains, LES data is used to feed RANS calculations through the boundary condition. In the present RANS formulation, transient term is taken into account and the LES time scales are incorporated in the RANS domain without problems. The velocity fluctuation results commented previously, probe that mixing both time scales does not interfere in time-related quantities, but just rather the opposite, it improves them in the LES domain. Despite the improvement is much significant in the Smagorinsky case, the overall results are better with the VMS-WALE model. This leads us to conclude that having a proper LES model is as necessary as having a well resolved near wall zone through the wall model.

5. The Ahmed Car test.

The standard benchmark case of the Ahmed Car has been computed at Reynolds Number $Re = 7 \times 10^5$, based on the inlet velocity, the vehicle height and the fluid viscosity. The slant angle of the back surface is 25°. The case has been selected because of the similarity of its flow characteristics with an stalled airfoil, including boundary layer detachment and flow recirculations. Mean velocity profile measurements in the recirculation zone were available unlike the DU-93-W-210 airfoil. A coarse mesh of 1.7×10^5 control volumes (CV) has been used in order to check the dynamic wall performance. Two cases have been performed, both using the WALE as a subgrid-scale model. In the first one, the dynamic wall model has been used while in the second one, only the LES model has been applied. In the case that uses the wall model, the wall domain mesh is extruded in 40 layers.

5.1. The Ahmed Car test results.

On figure 6, the mean velocity profiles obtained with and without the dynamic wall model are shown. These results have been obtained with a mesh of 1.7×10^5 CV. The results are plotted at different stream-wise positions. Finally, numerical results are compared with experimental ones provided by Erlangen University (Nuremberg).

On the other hand, on figure 7, the same numerical results obtained with the coarse (with and without wall model) are compared with results obtained by using a finer mesh of 1×10^6 CV [13]. This plot allows us to evaluate the performance of the wall model by comparing the results between two cases with identical meshes but with different wall treatment, and another case that uses a much finer mesh but without wall model.

5.2. Conclusions from the Ahmed Car test.

In the cases performed with the coarse mesh, it can be observed in figure 6 that the numerical results fit much better the experimental ones when the wall model is working. On the other hand, in figure 7, when comparing the coarse mesh results with the fine mesh ones, this improvement is also highlighted. Similar results are obtained in the modeled wall LES with coarse mesh if compared to the ones that have been obtained without wall model but using a six times finer grid. Hence, it can be concluded that in this case, the use of the dynamic wall model causes a significant improvement of the results.

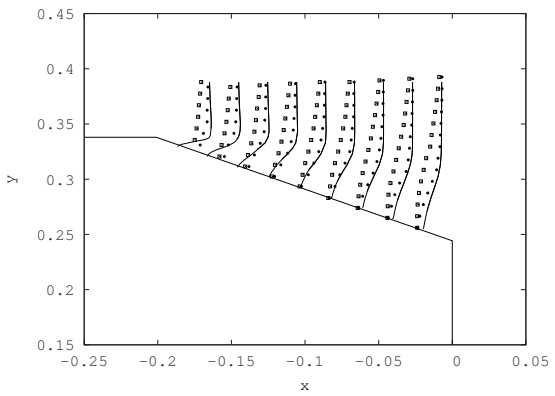

Figure 6. Comparison between mean velocity profiles obtained with a mesh of 1.7×10^5 CV with and without wall model, and experimental results. Numerical results are obtained by means WALE LES model. ● LES w/ wall model, □ LES w/o wall model,—— experimental.

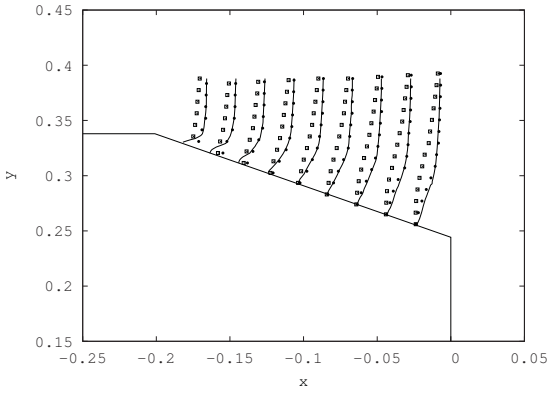

Figure 7. Comparison between mean velocity profiles obtained with a mesh of 1.7×10^5 CV with and without wall model, and results obtained with a mesh of 1×10^6 CV without wall model. All numerical results are computed with the WALE LES model. ● 1.7×10^5 CV LES w/ wall model, □ 1.7×10^5 CV LES w/o wall model,——1×10^6 CV LES w/o wall model

6. The DU-93-W-210 wind turbine dedicated airfoil case.

The DU-93-W-210 wind turbine airfoil, has already been studied in previous works [14] at various angles of attack (AoA) and at Reynolds number of $Re = U_0 c/\nu = 3 \times 10^6$, where U_0 is the free stream velocity, c is the airfoil chord and ν is the fluid viscosity. In those previous works, a fine mesh of 19×10^6 CV was used together with the VMS-WALE as a subgrid-scale model. Very good agreement with experimental results was obtained with this strategy. The main objective of the present work, as done in previous sections, is to evaluate the performance of the dynamic wall model. That is why in this study, a much coarser mesh of 3.9×10^6 CV has been used both applying and not applying the wall model. The AoA of 15° has been selected because at this position the airfoil is in stall condition and the wall model can be tested when strong boundary layer detachment and flow recirculations are present. As a LES model, the same VMS-WALE model has been applied. In figure 8, a snapshot of the fine and coarse meshes is displayed. In the figure on the right, the embedded wall mesh can be observed together with the coarse LDM.

6.1. The DU-93-W-210 case results.

In table 2 the lift and drag coefficient results are shown at $Re = 3 \times 10^6$ and $AoA = 15°$. A comparison between experimental data provided by Delft University of Technology (DUT) [15] and numerical results is done. The numerical values have been obtained using both, the fine (19×10^6 CV) and the coarse (3.9×10^6 CV) meshes. In the latest case, the coefficients have been obtained with and without wall model.

In figures 9 and 10, the numerical pressure and the skin friction coefficients are plotted along the airfoil chord. These results have been obtained with the coarse mesh by using and not using the dynamic wall model. Finally, in figures 11 and 12, the distance between the wall and the first off-wall node in wall units (y^+_{1n}) is shown. In figure 11, y^+_{1n} distribution is shown for the 3.9×10^6 coarse mesh while in figure 12 the same quantity is displayed but for the wall domain mesh.

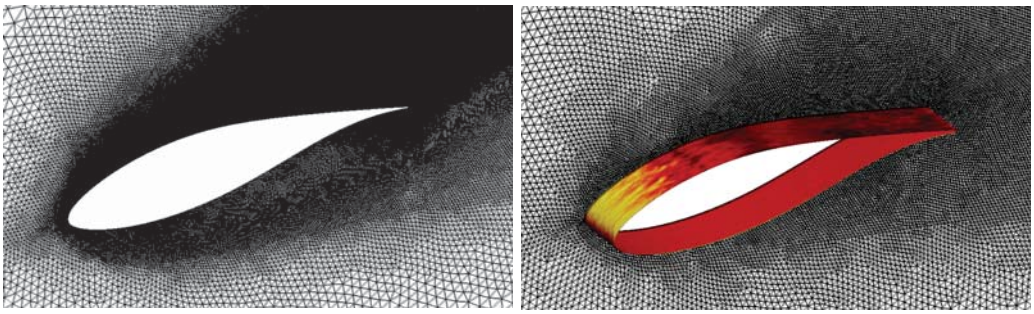

Figure 8. On the left, a DU-93-W-210 mesh of 19×10^6 CV used in previous works [14] is shown. On the right, the current mesh of 3.9×10^6 is displayed together with the wall domain mesh.

Table 2. Comparison between experimental and numerical results of the DU-93-W-210 lift and drag coefficients at $AoA = 15°$ and $Re = 3 \times 10^6$. Numerical results have been obtained with a fine and a coarse mesh. The coarse mesh has been tested with and without wall model.

coef. type	ref. value [15]	fine	r.err[%]	coarse	r.err.[%]	coarse+WM	r.err.[%]
Lift C_l	1.22	1.25	2.45	1.07	12.29	1.09	10.65
Drag C_d	0.092	0.091	1.08	0.201	118.4	0.176	91.3

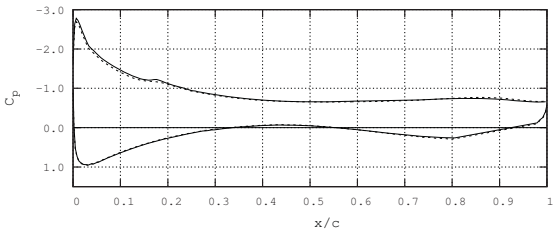

Figure 9. Pressure coefficient distribution along the upper and lower surface of the DU-93-W-210 airfoil at $Re = 3 \times 10^6$ and $AoA = 15°$. —— coarse mesh w/ wall model, - - - - coarse mesh w/o wall model

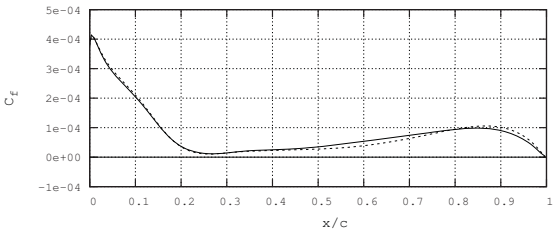

Figure 10. Skin friction coefficient distribution along the upper surface of the DU-93-W-210 airfoil at $Re = 3 \times 10^6$ and $AoA = 15°$. —— coarse mesh w/ wall model, - - - - coarse mesh w/o wall model

7. General conclusions.

The dynamic wall model has been tested with the reference cases of Channel Flow and Ahmed Car tests of which reference results were available. In both cases it has been proved that the model improves the LES results when using coarse meshes. Afterwards, a very unresolved DU-93-W-210 airfoil at $Re = 3 \times 10^6$ and at $AoA = 15°$ has been simulated. At some points of the LDM, the first off-wall node in the upper surface of the airfoil was far beyond $y^+ = 100$, this is well above the viscous sub layer. Due to the mesh coarseness, the LES results do not match the experimental ones. However when using the dynamic wall mesh, a slight improvement in lift coefficient is achieved as observed in table 2. Regarding the drag coefficient, the improvement is more significant. Slight differences in pressure and skin friction coefficients are observed in figures 9 and 10 but these variations caused by the use of the wall model, are in the right

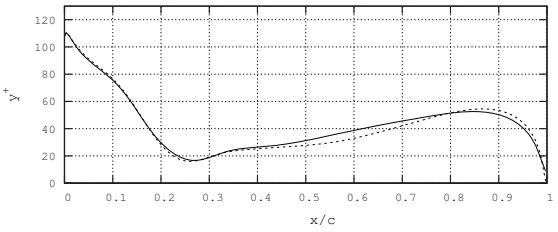

Figure 11. Distance between the wall and the first off-wall node in wall units. Distribution along the upper surface of the DU-93-W-210 airfoil at $Re = 3 \times 10^6$ and $AoA = 15°$. —— coarse mesh w/ wall model, - - - - coarse mesh w/o wall model.

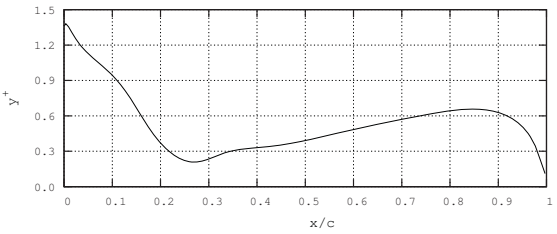

Figure 12. Distance between the wall and the first off-wall node of the wall model domain mesh in wall units. Distribution along the upper surface of the DU-93-W-210 airfoil at $Re = 3 \times 10^6$ and $AoA = 15°$.

direction as the aerodynamic coefficient values indicate. The improvement of the LES results is not as significant as the one achieved in the other testing cases. Despite the first off-wall node of the wall domain mesh is located at $y^+ = 1.35$, further studies analyzing the influence of the number of WDM layers will be carried out as well as different combinations of turbulence models both, in the LES and in the WDM-RANS domains.

References

[1] Wang M and Moin P 2002 Dynamic wall modeling for large-eddy simulation of complex turbulent flows *Phys. Fluids.* **14** N7 2043-51
[2] Lehmkuhl O, Rodríguez I, Baez A, Oliva A and Pérez-Segarra C D 2013 On the large-eddy simulations for the flow around aerodynamic profiles using unstructured grids *Comput. Fluids.* **84** 176-189
[3] Smagorinsky J 1963 General circulation experiments with the primitive equations, i. the basic experiment. *Mon. Weather Rev.* **91** 99-164
[4] Nicoud F and Ducros F 1999 Subgrid-scale stress modelling based on the square of the velocity gradient tensor *Flow. Turbul. Combust.* **62** 183-200
[5] Hughes T J R, Mazzei L and Jansen K E 2000 Large eddy simulation and the variational multiscale method *Comput. Vis. Sci.* **3** 47-59
[6] Vreman A W 2004 The adjoint filter operator in large-eddy simulation of turbulent flow *Phys. Fluids.* **16** 2012
[7] Verstappen R W C P and Veldman A E P 2003 Symmetry-preserving discretization of turbulent flow *J. Comput. Phys.* **187** 343-368
[8] Lehmkuhl O, Rodríguez I, Borrell R and Oliva A 2013 Low-frequency unsteadiness in the vortex formation region of a circular cylinder. *Phys. Fluids.* **25** 085109
[9] Rodríguez I, Borrell R, Lehmkuhl O, Prez-Segarra C D and Oliva A 2011 Direct numerical simulation of the flow over a sphere at Re = 3700 *J. Fluid Mech.* **679** 263-287
[10] Spalart P R and Allmaras S R 1944 A One-Equation Turbulence Model for Aerodynamic Flows *Rech. Aerospatiale.* **1** 5-21
[11] Pope S B 2000 *Turbulent Flows* (Cambridge: Cambridge University Press)
[12] Hoyas S and Jiménez J 2008 Reynolds number effects on the Reynolds-stress budgets in turbulent channels *Phys. Fluids.* **20** 101511
[13] Aljure D E, Rodríguez I, Lehmkhul O, Borrell R and Oliva A 2012 Flow and turbulent structures around simplified car models. *Proc. Conf. on Modelling fluid flow CMFF'12 (Budapest)* p 247-254
[14] Calafell J, Lehmkhul O, Rodríguez I and Oliva A 2012 On the Large-Eddy Simulation modelling of wind turbine dedicated airfoils at high Reynolds numbers *Proc. of the* 7^{th} *Int. Symp. on turbulence, heat and mass transfer* (ICHMT digital library/Begell House)
[15] Timmer W A and Van Rooij R P J O M 2004 Summary of the Delft University Wind Turbine Dedicated Airfoils *J. Sol. Energ.-T. ASME* **125**(4) 1-11